STEM CELLS®

TRANSLATIONAL AND CLINICAL RESEARCH

Glioma-Associated Stem Cells: A Novel Class of Tumor-Supporting Cells Able to Predict Prognosis of Human Low-Grade Gliomas

EVGENIA BOURKOULA,[a] DAMIANO MANGONI,[a] TAMARA IUS,[b,c] ANJA PUCER,[a] MIRIAM ISOLA,[a] DANIELA MUSIELLO,[a] STEFANIA MARZINOTTO,[a] BARBARA TOFFOLETTO,[a] MARISA SORRENTINO,[a] ANITA PALMA,[a] FEDERICA CAPONNETTO,[a] GIORGIA GREGORACI,[a] MARCO VINDIGNI,[b] STEFANO PIZZOLITTO,[d] GIOVANNI FALCONIERI,[d] GIOVANNA DE MAGLIO,[d] VANNA PECILE,[e] MARIA ELISABETTA RUARO,[a] GIORGIA GRI,[a] PIETRO PARISSE,[f] LOREDANA CASALIS,[f] GIACINTO SCOLES,[a] MIRAN SKRAP,[b] CARLO ALBERTO BELTRAMI,[a] ANTONIO PAOLO BELTRAMI,[a] DANIELA CESSELLI[a]

Key Words. Human glioma • Glioma-associated stem cells • Personalized medicine • Low-grade glioma • Prognostic score • Exosomes

[a]Department of Medical and Biological Sciences, University of Udine, Udine, Italy; [b]Department of Neurosurgery and [d]Department of Pathology, Azienda Ospedaliero-Universitaria of Udine, Udine, Italy; [c]Department of Robotics, Brain and Cognitive Sciences, Italian Institute of Technology, Genoa, Italy; [e]S.C. Medical Genetics, Institute for Maternal and Child Health; IRCCS "Burlo Garofolo", Trieste, Italy; [f]Sincrotrone Elettra Nano-Innovation Lab, Area Science Park, Basovizza, Trieste, Italy

Correspondence: Daniela Cesselli, M.D., Ph.D., Istituto di Anatomia Patologica, Piazzale S. Maria della Misericordia 15, 33100 Udine, Italy. Telephone: 39-0432559477; Fax: 39-0432559420; e-mail: daniela.cesselli@uniud.it

Received June 3, 2013; accepted for publication November 16, 2013; first published online in STEM CELLS *EXPRESS* December 4, 2013.

1066-5099/2014/$30.00/0

http://dx.doi.org/10.1002/stem.1605

ABSTRACT

***Background*: Translational medicine aims at transferring advances in basic science research into new approaches for diagnosis and treatment of diseases. Low-grade gliomas (LGG) have a heterogeneous clinical behavior that can be only partially predicted employing current state-of-the-art markers, hindering the decision-making process. To deepen our comprehension on tumor heterogeneity, we dissected the mechanism of interaction between tumor cells and relevant components of the neoplastic environment, isolating, from LGG and high-grade gliomas (HGG), proliferating stem cell lines from both the glioma stroma and, where possible, the neoplasm. *Methods and Findings*: We isolated glioma-associated stem cells (GASC) from LGG (n=40) and HGG (n=73). GASC showed stem cell features, anchorage-independent growth, and supported the malignant properties of both A172 cells and human glioma-stem cells, mainly through the release of exosomes. Finally, starting from GASC obtained from HGG (n=13) and LGG (n=12) we defined a score, based on the expression of 9 GASC surface markers, whose prognostic value was assayed on 40 subsequent LGG-patients. At the multivariate Cox analysis, the GASC-based score was the only independent predictor of overall survival and malignant progression free-survival. *Conclusions*: The microenvironment of both LGG and HGG hosts non-tumorigenic multipotent stem cells that can increase *in vitro* the biological aggressiveness of glioma-initiating cells through the release of exosomes. The clinical importance of this finding is supported by the strong prognostic value associated with the characteristics of GASC. This patient-based approach can provide a groundbreaking method to predict prognosis and to exploit novel strategies that target the tumor stroma.** STEM CELLS *2014;32:1239–1253*

INTRODUCTION

Gliomas, the most frequent malignant primitive tumors of the central nervous system [1], can be divided, according to WHO classification, into high-grade gliomas (grades 3 and 4, HGG) and low-grade gliomas (grades 1 and 2, LGG) [2]. Although relatively rare (incidence of 5/100,000 person/years in Europe and North America), HGG are associated, despite optimal treatment, with disproportionately high morbidity and mortality [3], while LGG grow slowly, but approximately 70% of grade 2 gliomas evolves to anaplasia, in turn leading to neurological disability and ultimately to death, within 5–10 years [4–6]. However, both LGG and HGG are characterized by a wide clinical heterogeneity and histological analyses, even when combined with newly identified molecular markers, partially fail in predicting the clinical evolution of the lesions [7–10]. Therefore, to profoundly impact the outcome of glioma patients, new drugs and better prognostic/predictive factors are strongly required.

The isolation and characterization of glioma stem cells (GSC) have opened new insights into glioma biology offering the unique possibility to study, and possibly target, the rare population of cells responsible for tumor development, relapse, and drug-resistance [11–13]. However, GSC have been identified only in a fraction of HGG and seldom in adult LGG [14], they are rare and difficult to expand in culture, thus making a challenge the use of these cells to identify novel therapies and biomarkers.

Table 1. Clinicopathologic features of the $n = 113$ patients whose glioma tissues were used to isolate stem cells

Grade	*n*	Male *n* (%)	Age_years (mean ± SD)	Histopathological diagnosis
Low grade	40	25 (62.5%)	38 ± 12	Diffuse astrocytoma ($n = 22$) Oligoastrocytoma ($n = 11$) Gemistocytic astrocytoma ($n = 3$) Oligodendroglioma ($n = 3$) Pleomorphic xanthoastrocytoma ($n = 1$)
High grade	73	41 (56%)	59 ± 12	Glioblastoma multiforme ($n = 56$) Anaplastic astrocytoma ($n = 9$) Gliosarcoma ($n = 5$) Giant cell glioblastoma ($n = 3$)
p	–		$p < .0001$	

Lately, a great interest has been aroused by the tumor-associated microenvironment. This latter, which consists of multiple distinct cell types, including tumor-associated fibroblasts (TAF) [15, 16], plays, in most carcinomas, an active role in tumor proliferation, invasion, and metastasis [17–19]. Intriguingly, some biological characteristics of the stromal elements of tumors may be of prognostic and predictive value, and they could offer novel targeting opportunities [17–20]. Moreover, it has been recently shown that, in the tumor, both cancer cells and tumor-associated stromal cells promote tumor-induced immune suppression, angiogenesis, and metastasis through the release of exosomes [21–24]. These latter are membrane vesicles that originate in multivesicular bodies and are released in the extracellular space and in the body fluids from many cell types [24–26] and, through their content in biologically active molecules (e.g., proteins, mRNAs, and miRNAs), they act as a potent intercellular communication system [24–26]. Regarding gliomas, although some experimental evidences support the role played by the microenvironment in controlling the course of pathology [27, 28], the correlation between the biological characteristics of the first one with the clinical outcome of patients has never been investigated.

In this article, we isolated for the first time, both from LGG and HGG, a population of stem cells characterized by tumor-supporting activities, being able, through the release of exosomes, to increase the biological aggressiveness of glioma-initiating cells. Importantly, the in vitro features of these cells, named GASC (glioma-associated stem cells), were the strongest predictor of LGG patients' overall survival (OS) and malignant progression-free-survival (MPFS) outperforming the state-of-the-art prognostic factors.

Materials and Methods

Detailed Supporting Information Methods are available online.

The independent ethic committee of the Azienda Ospedaliero-Universitaria of Udine has approved the research. Informed consents have been obtained from patients and all clinical investigations have been conducted according to the principles expressed in the Declaration of Helsinki.

Supporting Information Table S1 summarizes the sampling size of each experiment performed.

Tissue Donors

Cells were isolated from 113 patients affected by a supratentorial glioma arising de novo. All patients, not treated with neo-adjuvant therapy, underwent surgical resection in the period June 2006 to March 2011 (Tables 1 and 2).

Histological Examination, Immunohistochemistry, FISH, and Analysis of the Genetic Status of MGMT and IDH Genes

Tumors were histopathologically reviewed according to WHO classification [2]. Mitotic index, Ki-67, p53, glial fibrillary acidic protein (GFAP) (Dako Denmark A/S, Glostrup, Denmark, http://www.dako.com), Epidermal Growth Factor Receptor (EGFR) (Zymed Laboratories, Invitrogen, Carlsbad CA, http://www.lifetechnologies.com), and $IDH1^{R132H}$ (Dianova, Hamburg/Germany, http://www.dianova.com) were detected on 4-μm-thick formalin-fixed paraffin-embedded sections. Fluorescence In Situ Hybridization (FISH) analysis was performed using dual-color 1p36/1q25 and 19q13/19p13 probes (Vysis, (Vysis, Abbott Molecular, Illinois, IL, U.S.A, http://www.abbottmolecular.com)). IDH1 and IDH2 gene status were evaluated by pyrosequencing as in [29]. Levels of the MGMT promoter were investigated by PyroMark Q96-CpG-MGMT (Quiagen, Hilden, Germany http://www.qiagen.com/). See Supporting Information methods.

Volumetric Analysis

All preoperative and postoperative (4 months) tumoral segmentations were performed manually across all magnetic resonance imaging slices with the OSIRIX software tool to measure tumor volumes (cm^3) on the basis of T2 axial slices, as in [30, 31].

GASC Isolation and Culture

Cells from glioma were isolated and cultured applying, with minor modifications, previously described protocols [32–34]. Briefly, glioma fragments were mechanically enzymatically dissociated and cells less than 40 μm in diameter were cultured in expansion medium as in [32–34]. See Supporting Information methods for details.

Isolation and Culture of GSC in Adhesion

Cells after mechanic-enzymatic digestion were cultured on laminin-coated dishes in a neural stem cell medium as in [13]. See Supporting Information methods for details.

Flow-Cytometry

After enzymatic detachment, cells were incubated with properly conjugated or unconjugated antibodies. The analysis was performed either by FACS-Calibur, FACScanto (BD Biosciences, San Jose, CA, http://www.bdbiosciences.com), or by CyAn (Beckman Coulter s.r.l., Milan, Italy, https://www.beckmancoulter.com)

[32–34]. Exosome staining was performed after incubation of exosomes with 4 μm aldehyde/sulfate latex beads (Molecular Probes, Invitrogen, Carlsbad CA, http://www.lifetechnologies.com). See Supporting Information methods for details.

Immunofluorescence

Cell staining and image acquisition were conducted as in [32–34]. See Supporting Information Methods for details.

Reverse Transcriptase PCR Analysis

Total RNA was extracted from P_3-GASC using the TRIzol Reagent (Invitrogen, Carlsbad CA, http://www.lifetechnologies.com) [34]. First strand cDNA synthesis, PCR amplification, and analysis of reaction products were performed as in [34]. See Supporting Information Table S2 for primer pairs and product length.

Cell Culture Assays

Cell growth kinetic, single-cell cloning, multilineage differentiation, and functional assays were performed as in [32–35]. See Supporting Information methods for details.

Soft Agar Assay

Cells were plated in a 0.25% soft agar solution in plates containing a basal layer of 1% agarose. The effects of exosomes on GSC have been evaluated by CytoSelect 96-well Cell Transformation Assay (Cell Biolabs Inc., San Diego, CA, http://cellbiolabs.com). See Supporting Information methods for details.

Single Nucleotide Polymorphism (SNP) Analysis

SNP array analysis was carried out using the Infinium high-density HumanCytoSNP-12 DNA analysis BeadChips (Illumina United Kingdom, Essex, UK, http://www.illumina.com). Data analysis was performed using the Illumina GenomeStudio v.2010 software. See Supporting Information methods for details.

Exosomes for A172 Conditioning

Culture supernatants conditioned for 48 hours by 6×10^6 cells were collected and split in aliquots. One of these was diluted 1:1 with ultracentrifuged DMEM (uDMEM) (Gibco, Invitrogen, Carlsbad, CA, http://www.lifetechnologies.com) (SN+). The other one was used for exosomes purification by ExoQuick-TC (System Biosciences, Mountain View, CA, http://www.systembio.com). The exosome-depleted culture supernatant was diluted 1:1 with uDMEM (SN−). The exosome pellet was resuspended in the same volume of uDMEM (EXO). Before functional assays, A172 were cultured for at least two passages in the different media. See Supporting Information methods for details.

Exosomes for GSC Conditioning

Exosomes produced in 48 hours by 6×10^6 cells were precipitated by ExoQuick-TC (System Biosciences, Mountain View, CA, http://www.systembio.com) and resuspended in 40 ml of neural stem cell medium. Before functional assays, GSC were cultured in exosomes-enriched media for one passage. See Supporting Information methods for details.

Atomic Force Microscopy

Exosomes were adsorbed to freshly cleaved mica sheets and analyzed by MFP-3D Stand Alone Atomic Force Microscopy (AFM) (Asylum Research, Mannheim, Germany, www.asylumresearch.de) in dynamic mode with silicon probes (Force constant 0.5–1 N/m, radius of curvature <10 nm, Mikromasch, Wetzlar, Germany, http://www.nanoandmore.com). See Supporting Information methods for details.

Exosome Internalization Assay

A172 cells were incubated for 4 hours in Dulbecco's modified Eagle's medium (DMEM) added with exosomes labeled by DiD (Molecular Probes Invitrogen, Carlsbad, CA, http://www.lifetechnologies.com). Cells were fixed, stained with TRITC-labeled phalloidin (Sigma-Aldrich, St. Louis, MO, United States http://www.sigmaaldrich.com), and fluorescence images acquired either by Leica TCS SP2 confocal microscope or by Leica DMI600B epifluorescence microscope equipped with a deconvolution software (Leica AF6000, Leica Microsystems, Wetzlar, Germany, http:// leica.com).

Scratch Assay

Cells were plated onto 96-well high-content imaging plates (Becton Dickinson Diagnostic Systems, Sparks, MD, http://www.bd.com/). At confluence, cell monolayers were scraped with a p10 pipette tip. Images of the "scratches" were acquired at specified time intervals. See Supporting Information methods for details.

Statistical Analysis

Characteristics of the study population are described using standard methods. In order to define a risk profile for LGG patients we adopted a multistep approach (Supporting Information Fig. S1). OS, PFS (progression-free survival), and MPFS were defined as time between initial surgery and, respectively, death (OS), demonstration of unequivocal increase in tumor size on follow-up imaging, malignant progression, and/or death (PFS), and demonstration of gadolinium enhancement on follow-up imaging and/or higher-grade tumor on subsequent biopsy or death (MPFS).

OS, PFS, and MPFS were described using the Kaplan-Meier approach. Analysis of survival was done using Cox proportional hazard models. Covariates with $p < .05$ at univariable analysis were selected for multivariable stepwise analysis. See Supporting Information methods for details.

Results

Isolation of GASC from LGG and HGG

To establish whether human gliomas possess a population of stem cells with tumor-supporting ability, we applied the method, previously optimized to isolate multipotent adult stem cells (MASC) from normal [32, 33] and neoplastic tissues [34], to 113 de novo supratentorial glioma samples. These latter were grouped as LGG ($n = 40$) or HGG ($n = 73$), based on the histological diagnosis (Table 1). Once tumor fragments (weighing an average of 125 mg) were digested, dissociated cells were cultured in a medium selective for the growth of MASC [32–34]. Only a minority of the seeded cells was able to adhere and proliferate, and the colony-forming efficiency was lower for cells obtained from HGG with respect to those obtained from LGG (Supporting Information Fig. S2A–S2D). Despite the stringent culture conditions, 5–7 days after the primary culture, proliferating cell lines were obtained in

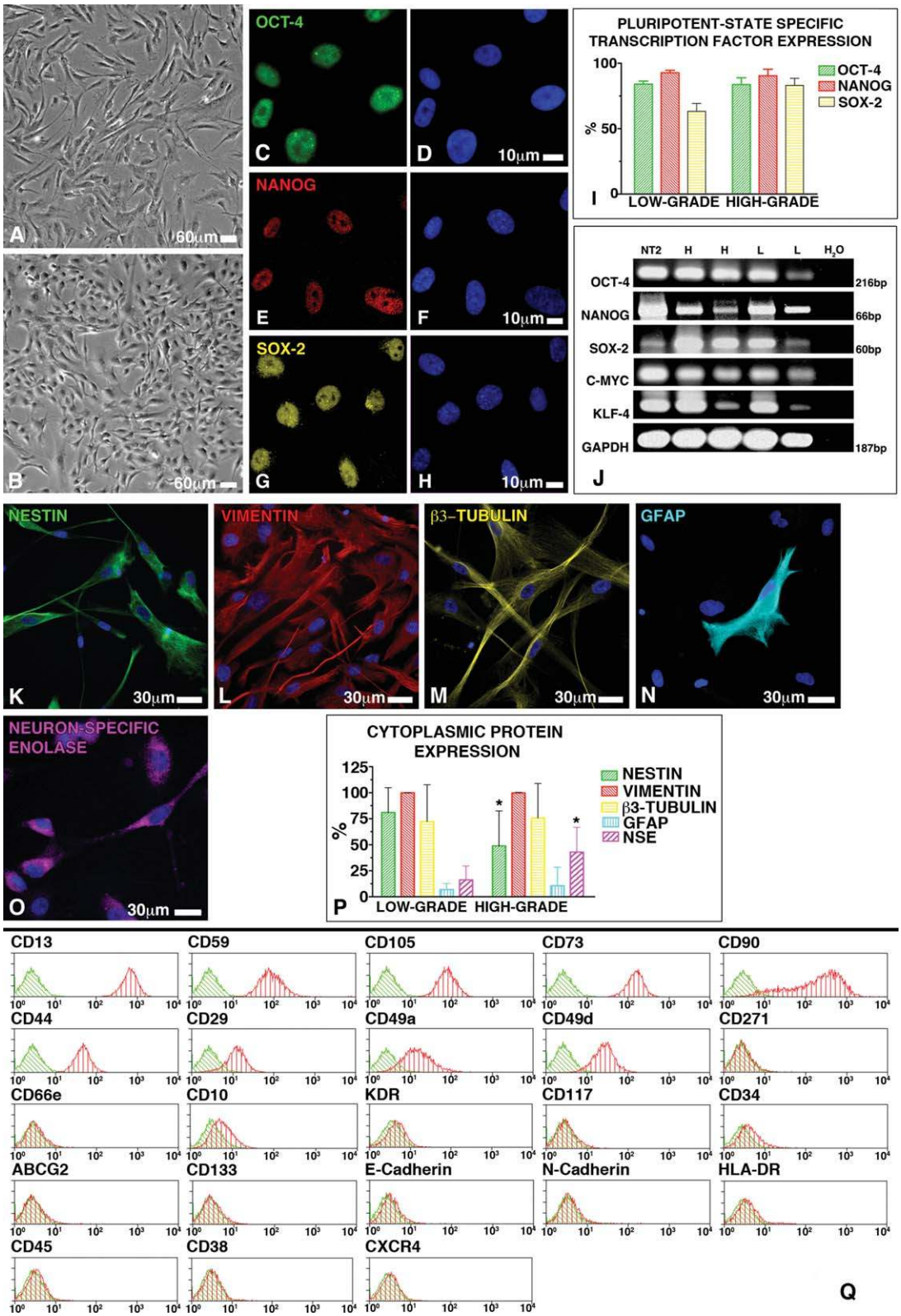

Figure 1. Features of glioma-associated stem cells (GASC) at the third passage in culture. **(A, B):** Phase-contrast image of GASC obtained from human low-grade gliomas (A) and high-grade gliomas (B). **(C–J):** Pluripotent state-specific transcription factor expression. GASC express Oct-4 (green fluorescence, C, D), Nanog (red fluorescence, E, F), and Sox-2 (yellow fluorescence, G, H). In D, F, and H, nuclei are depicted by the blue fluorescence of DAPI staining. (I): Results are presented as mean ± SD. (J): Transcripts for OCT3/4, NANOG, SOX2, KLF4 c-MYC, and GAPDH are present in GASC obtained from low-grade (L) and high-grade (H) glioma samples. The neuronally committed human teratocarcinoma cell line (NT2) was used as positive control. **(K–P):** Cytoplasmic protein expression in GASC. Expression of nestin (green fluorescence, K), vimentin (red fluorescence, L), beta three tubulin (yellow fluorescence, M), GFAP (cyan fluorescence, N), and neuron-specific enolase (magenta fluorescence, O) in GASC. Nuclei are depicted by the blue fluorescence of DAPI staining. (P): Results are presented as mean ± SD. *, $p < .05$ versus low-grade glioma derived-GASC. **(Q):** Representative surface immunophenotype of GASC. Histograms overlays show isotype control IgG staining profile (green histograms) versus specific antibody staining profile (red histograms). Abbreviation: GFAP, glial fibrillary acidic protein.

approximately 95% of both LGG and HGG, confirming the high efficiency of the optimized method [32–34].

Since 1 week from seeding, proliferating cells were highly positive for the expression of the intermediate filaments characterizing an undifferentiated state, such as vimentin and nestin, as well as of pluripotent-state-specific transcription factors Oct-4 and Nanog (Supporting Information Fig. S2E–S2J), thus excluding that the acquisition of these features could be related to an extensive culture manipulation. Conversely, the GFAP was expressed only in a minority of the cells (Supporting Information Fig. S2I–S2J). Because of the stem cell features, we named these proliferating cell lines GASC, defining as L-GASC and H-GASC those obtained from LGG and HGG, respectively.

L-GASC and H-GASC Displayed Stem Cell Properties

L- and H-GASC at the third passage in culture shared a fibroblast-like morphology (Fig. 1A, 1B) and an undifferentiated state, as assed by Oct-4, Nanog, Sox-2, Klf-4, c-Myc, vimentin, and nestin expression (Fig. 1C–1L, 1P) and the low positivity for GFAP (Fig. 1N, 1P). However, these cell types differed in the expression of neuron-specific enolase and nestin (Fig. 1O, 1P). The growth kinetic of H- ($n = 18$) and L-GASC ($n = 27$) did not differ significantly, being the population doubling time (PDT) 34 ± 18 versus 37 ± 13 hours, respectively ($p > .05$).

Flow-cytometry analysis of the surface immunophenotype demonstrated that, despite some significant differences (Supporting Information Table S3), L- and H-GASC shared a similar mesenchymal phenotype (Fig. 1Q). H-GASC showed, with respect to L-GASC, an increased expression of CD90, ABCG2, CD133, CD66e, E-Cadherin, KDR, and significantly lower levels of CD105 and CD44 (Supporting Information Table S3).

In order to test whether GASC were characterized by stem cell properties, a single-cell cloning assay was performed ($n = 3$ L-GASC and $n = 3$ H-GASC). Of 2,041 seeded GASC, 452 gave rise to highly proliferating clones (Fig. 2A–2C). Importantly, clonal cells maintained a stable undifferentiated phenotype (Fig. 2D, 2E, 2G, 2H, 2J).

When cultured under appropriate differentiation inducing conditions, clonal GASC (at least $n = 5$ from both LGG and HGG) acquired lineage-specific features, without significant differences between HGG- and LGG-derived clones (data not shown). Globally, clones exposed to neural differentiation medium displayed a morphological change (Fig. 2F), a decreased expression of both nestin and pluripotent-state-specific transcription factors (Fig. 2G–2J), and the acquisition of the neuronal-specific markers synaptophysin and MAP-2 (Fig. 2K, 2L, 2P), of the glial-specific marker GFAP (Fig. 2N, 2P) and of the oligodendrocyte marker O4 (Fig. 2O, 2P). Only a small fraction of cells grown in a medium added with GM-CSF and conditioned by astrocytes acquired phenotypical and functional microglial properties, as being positive for the microglial markers Iba-1, coexpressing CD11b and CD45 and characterized by phagocytic activity (Fig. 2Q–2T). Similarly to MASC isolated from normal tissues [32, 33, 36], GASC retain the ability to differentiate along mesodermic derivatives, such as endothelial- (Fig. 2U-W), osteoblast-, and myocyte-like cells, and endodermic derivatives, such as hepatocyte-like cells, although with a low efficiency (Supporting Information Fig. S3). Altogether, the accumulated evidences showed that it is possible to isolate from glioma samples a population of cells characterized by a mesenchymal stem cell phenotype, clonogenicity, and multipotency, similarly to what has already been demonstrated for non-neoplastic human tissues.

GASC Possess Aberrant Growth Properties but Are Not Tumorigenic

Despite some similarities, the growth properties of L- and H-GASC were significantly different from those of MASC obtained from normal tissues [32, 33, 36].

Specifically, when cultured in soft agar, H- and L-GASC displayed an anchorage-independent growth (Fig. 3A–3C). This aberrant growth property increased upon in vitro expansion (Fig. 3C) and was further retained by GASC even after single-cell cloning ($n = 6$; Fig. 3D, 3E), demonstrating the ability of the used culture conditions to preserve the atypical features of GASC.

Despite their ability to grow in semisolid medium, L- and H-GASC significantly differed from glioma-initiating cells. In fact, when GASC isolated from HGG were compared with the GSC obtained following the protocol optimized by Dirks's group to expand GSC in adherent culture [13] (Fig. 3F), several differences became apparent. Because of the described inefficiency in growing GSC from adult LGG [14], we limited our analysis to HGG. Although both GSC and H-GASC expressed nestin, Nanog, Oct-4, and Sox-2 (Fig. 3G–3J), only GSC were significantly enriched in the GSC markers CD133 and CD117 [37], as well as in N-cadherin (Fig. 3K), a protein involved in GSC migration [38]. The direct comparison of four GASC and four GSC obtained from the same four HGG patients, demonstrated that, although GSC tended to grow slower than GASC (Fig. 3L), only GSC spontaneously formed neurospheres, despite the use of laminin to favor an adherent growth (Fig. 3L). Additionally, GSC presented a superior anchorage-independent growth, giving rise, after 3 weeks of culture, to a larger number of bigger colonies (Fig. 3M). Importantly, when tested by FISH for genetic aberrations frequent in gliomas (i.e., aneuploidy of chromosomes 1 and 19), the majority of GSC showed abnormalities, mainly absent in the respective GASC (Fig. 3N).

The non-neoplastic nature of GASC was further confirmed by a whole genome SNP analysis ($n = 3$ L-GASC and $n = 1$ H-GASC) (Fig. 3O). Specifically, comparing the SNP profile of each GASC-line with the ones of the respective tumor of origin and of the mononuclear cells of the peripheral blood (negative control), all tested GASC were devoid of the genetic alterations characterizing the glioma tissues (Fig. 3O). Accordingly, when injected into the striatum of NOD-Scid mice ($n = 26$), 10^5 either polyclonal ($n = 12$) or clonal GASC ($n = 12$) were unable to give rise, even after 8 months, to tumors, while B2C cells ($n = 2$) did (data not shown). In conclusions, although GASC display aberrant growth properties in vitro, they differ from GSC, are devoid of the genetic alterations characterizing the glioma of origin, and are not able to originate a tumor when injected in vivo.

GASC Possess a Tumor-Supporting Phenotype Mediated by Exosomes

The aberrant growth displayed by GASC in the absence of genetic mutations strictly reminds the distinguishing features of TAF [39]. These latter are characterized by the ability to modify the biological properties of tumor cell lines in vitro. Therefore, we tested whether a medium semiconditioned by H-GASC possessed the ability to modify growth kinetics and adhesion-independent growth of the glioblastoma cell lines A172 and U87. When grown in a medium conditioned by H-

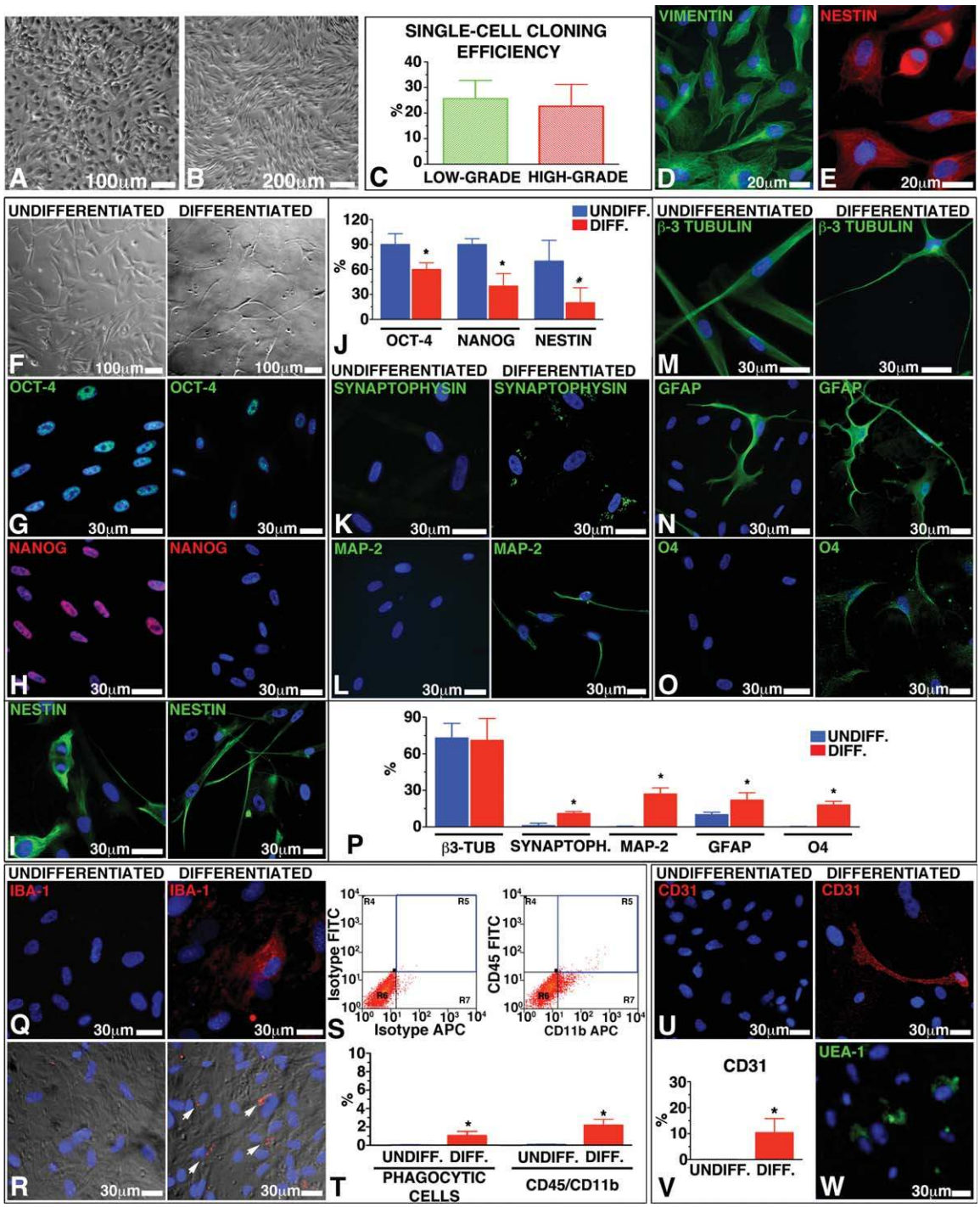

Figure 2. Clonogenicity and multipotency of glioma-associated stem cells (GASC). **(A–E):** Clonogenicity of GASC. (A, B): Phase-contrast images of single-cell derived clones of low-grade gliomas- and high-grade gliomas-derived cells. (C): Results are presented as mean ± SD. (D, E): Vimentin (green fluorescence, D) and nestin (red fluorescence, E) expression by GASC. Nuclei are depicted by the blue fluorescence of DAPI staining. **(F–X):** Multipotency of single GASC-derived clones. Neural differentiation: (F) phase-contrast pictures of undifferentiated GASC (left) and GASC differentiated into neural derivatives (right). (G–N): Oct-4 (green fluorescence, G), Nanog (red fluorescence, H), nestin (green fluorescence, I), synaptophysin (green fluorescence, K), MAP-2 (green fluorescence, L), beta3-tubulin (green fluorescence, M), GFAP (green fluorescence, N), and O4 (green fluorescence, O) expression in undifferentiated- (left panels) and differentiated- (right panels) GASC. Microglial differentiation: Iba-1 expression (red fluorescence, Q) and opsonized latex beads (red fluorescence, arrows, R) phagocytosis after PMA stimulation in undifferentiated- (left panels) and differentiated- (right panels) GASC. (S): Dot plots showing differentiated cells stained with both isotype-matched (left) and CD11b-APC and CD45-FITC antibodies (right). Endothelial differentiation: few GASC cultured in endothelial-inducing conditions became positive for CD31 (red fluorescence, U) and the lectin (UEA I, green fluorescence, W). Nuclei are depicted by the blue fluorescence of DAPI staining. (J, P, T, V): Results are expressed as mean ± SD. *, $p < .05$ versus undifferentiated. Abbreviations: GFAP, glial fibrillary acidic protein; UEA I, *Ulex europaeus* agglutinin I.

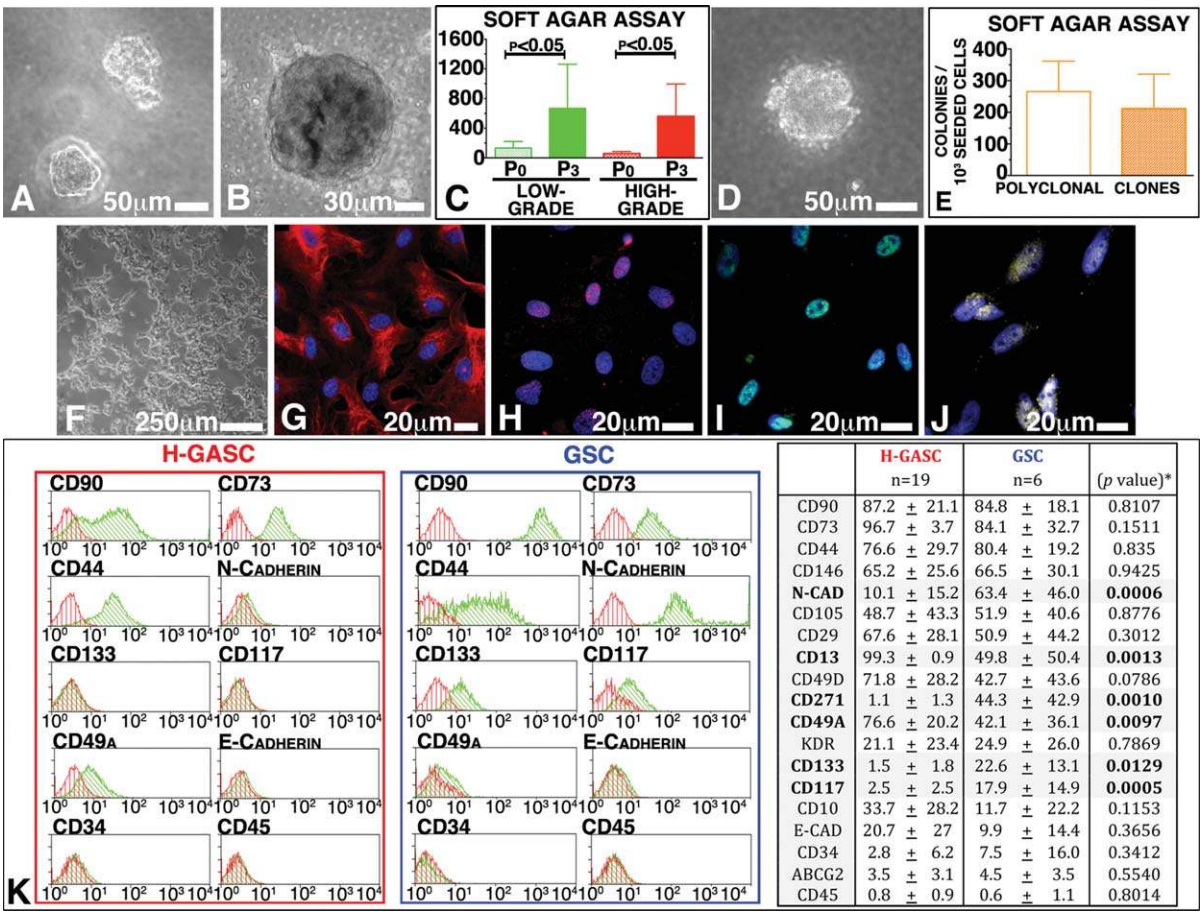

	H-GASC n=19	GSC n=6	(*p* value)*
CD90	87.2 ± 21.1	84.8 ± 18.1	0.8107
CD73	96.7 ± 3.7	84.1 ± 32.7	0.1511
CD44	76.6 ± 29.7	80.4 ± 19.2	0.835
CD146	65.2 ± 25.6	66.5 ± 30.1	0.9425
N-CAD	10.1 ± 15.2	63.4 ± 46.0	**0.0006**
CD105	48.7 ± 43.3	51.9 ± 40.6	0.8776
CD29	67.6 ± 28.1	50.9 ± 44.2	0.3012
CD13	99.3 ± 0.9	49.8 ± 50.4	**0.0013**
CD49D	71.8 ± 28.2	42.7 ± 43.6	0.0786
CD271	1.1 ± 1.3	44.3 ± 42.9	**0.0010**
CD49A	76.6 ± 20.2	42.1 ± 36.1	**0.0097**
KDR	21.1 ± 23.4	24.9 ± 26.0	0.7869
CD133	1.5 ± 1.8	22.6 ± 13.1	**0.0129**
CD117	2.5 ± 2.5	17.9 ± 14.9	**0.0005**
CD10	33.7 ± 28.2	11.7 ± 22.2	0.1153
E-CAD	20.7 ± 27	9.9 ± 14.4	0.3656
CD34	2.8 ± 6.2	7.5 ± 16.0	0.3412
ABCG2	3.5 ± 3.1	4.5 ± 3.5	0.5540
CD45	0.8 ± 0.9	0.6 ± 1.1	0.8014

Figure 3. GASC grow in soft agar but differ from GSC. **(A–E):** Anchorage-independent growth of GASC. Phase-contrast images of colonies in soft agar of low-grade gliomas- (A), high-grade gliomas- (B), GASC and of a single-cell-derived clone (D). (C): Quantification of the absolute number of colonies >100 μm in diameters formed after 30 days. (E): Number of colonies/1,000 seeded cells grown in soft agar of single-cell-derived clones versus the respective polyclonal cell lines ($n = 6$). In (C) and (E), results are expresses as mean ± SD. **(F–J):** GSC features. Phase-contrast picture (F), nestin (red fluorescence, G), Nanog (red fluorescence, H), Oct-4 (green fluorescence, I), and Sox-2 (yellow fluorescence, J) expression by GSC. Nuclei are depicted by the blue fluorescence of DAPI. **(K–M):** GASC versus GSC. (K): Surface immunophenotype: on the left, representative histograms overlays showing isotype control IgG staining profile (red histograms) versus specific antibody staining profile (green histograms); on the right, table comparing GSC versus H-GASC expression of 19 surface proteins. (L): Growth kinetic: nuclear density (blue fluorescence of DAPI) of H-GASC and GSC at 1 (i, iii) and 10 (ii, iv) days from seeding. While H-GASC grew as a monostrate (ii), GSC tended to spontaneously form neurospheres (arrow, iv; phase-contrast image, v). In vi, data are presented as mean ± SD. (M): Anchorage-independent growth: on the left, phase-contrast images of colonies growing in soft agar 3 weeks from seeding. On the right, results are expressed as mean ± SD. *, $p < .05$ versus GASC. **(N):** FISH analysis. Red dots identify 1p36 (i, ii) and 19q13 (iii, iv) while green dots 1q25 (i, ii) and 19p13 (iii, iv) in H-GASC (i, iii) and GSC (ii, iv), respectively. In v and vi, results are expressed as mean ± SD. *, $p < .05$ versus GASC. **(O):** SNP analysis. In the upper panel, data from Infinium high-density humanCytoSNP-12 DNA analysis BeadChips revealing a mosaic deletion of the chromosome 1p in the glioma tissue but not in the GASC obtained from it as well as in the peripheral blood cells of the same patient. In the lower panel, table summarizing the results of the four studied cases. II^A diffuse astrocytoma; II^B oligoastrocytoma; III anaplastic astrocytoma. Abbreviations: GASC, glioma-associated stem cells; GSC, glioma-initiating stem cell.

GASC ($n = 6$), both A172 and U87 displayed a significant decrease in the PDT and an increased ability to grow in soft agar (Supporting Information Fig. S4).

Since it has been recently demonstrate that stromal cells, such as TAF, can act through the release of exosomes [21, 40], we evaluated whether GASC could exert their tumor-supporting action in this way. Exosomes were isolated from H-GASC culture supernatants by ExoQuick-TC and their presence was confirmed both by fluorescence-activated cell sorting (FACS) (expression of CD9 and CD63, Fig. 4A) and AFM (particles with a diameter ranging from 20 to 110 nm, Fig. 4B). In order to establish whether recipient cells could internalize exosomes, A172 cells were incubated for 4 hours with Di-D-labeled exosomes and cells examined either by confocal microscopy or epifluorescence imaging followed by deconvolution. As shown in Figure 4C, DiD-labeled exosomes could be identified within the cells and the internalization was further confirmed by FACS (Fig. 4D).

Subsequently, we compared the capacity of unfractioned GASC supernatants (SN+), exosome-depleted GASC supernatants (SN−), and GASC-derived exosomes (EXO) to modify growth kinetic, migration ability, and anchorage-independent growth of A172 cells (Fig. 4E). These latter, when grown in GASC-SN+ and GASC-EXO, showed a significant decrease in the PDT (Fig. 4F) and a significant increase both in motility and anchorage-independent growth (Fig. 4G, 4H). These

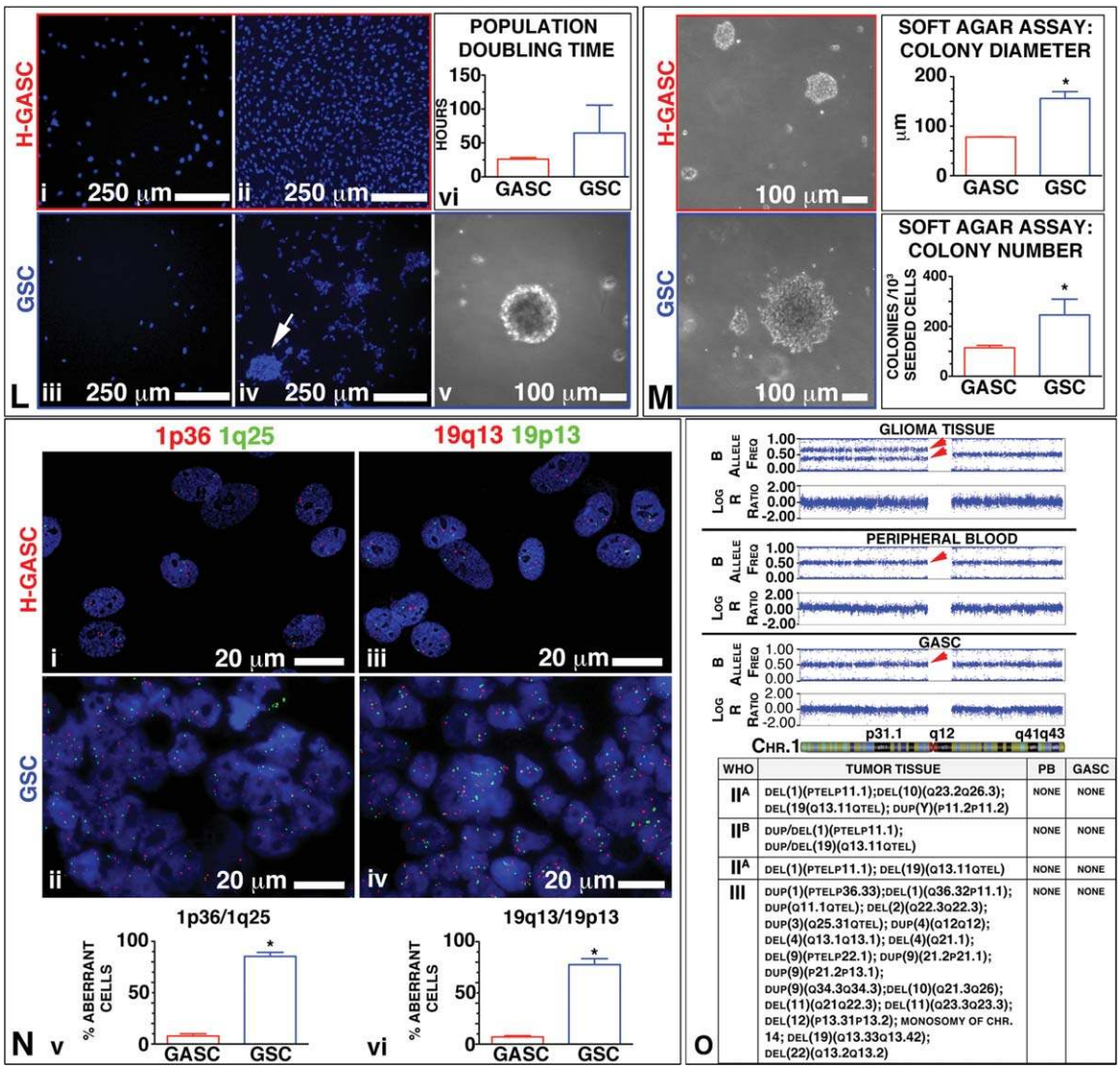

WHO	TUMOR TISSUE	PB	GASC
II^{A}	DEL(1)(PTELP11.1);DEL(10)(Q23.2Q26.3); DEL(19)(Q13.11QTEL); DUP(Y)(P11.2P11.2)	NONE	NONE
II^{B}	DUP/DEL(1)(PTELP11.1); DUP/DEL(19)(Q13.11QTEL)	NONE	NONE
II^{A}	DEL(1)(PTELP11.1); DEL(19)(Q13.11QTEL)	NONE	NONE
III	DUP(1)(PTELP36.33);DEL(1)(Q36.32P11.1); DUP(Q11.1QTEL); DEL(2)(Q22.3Q22.3); DUP(3)(Q25.31QTEL); DUP(4)(Q12Q12); DEL(4)(Q13.1Q13.1); DEL(4)(Q21.1); DEL(9)(PTELP22.1); DUP(9)(21.2P21.1); DUP(9)(P21.2P13.1); DUP(9)(Q34.3Q34.3);DEL(10)(Q21.3Q26); DEL(11)(Q21Q22.3); DEL(11)(Q23.3Q23.3); DEL(12)(P13.31P13.2); MONOSOMY OF CHR. 14; DEL(19)(Q13.33Q13.42); DEL(22)(Q13.2Q13.2)	NONE	NONE

Figure 3. (Continued).

changes were not present when A172 cells were grown in SN−, supporting the notion that exosomes were the main responsible for the effects observed. Importantly, Wi38 fibroblasts-EXO did not affect A172 cells (Fig. 4E–4H). Conversely, Wi38-SN+ reduced the growth of A172 cells, and this effect was mainly attributable to the nonexosomal component of the supernatant, thus supporting the notion that the effects of the GASC supernatant were cell- and exosomes dependent. Similarly to exosomes released by H-GASC, those obtained from L-GASC significantly affected PDT, anchorage-independent growth, and motility of A172, although at a significant lower extent (Fig. 4I–4K), thus suggesting that the degree of the tumor-supporting ability was proportional to the grade of malignancy of the tumor of origin. Finally, in order to assess the effects of GASC-exosomes on a clinically relevant experimental setting, we isolated, from three HGG patients, both H-GASC and GSC, and verified the effects of the H-GASC-exosomes on the respective GSC lines (Fig. 4L).

Exosomes obtained from H-GASC profoundly modified the growth pattern of GSC, which started to form tridimensional cords of cells loosely adherent to each other (Fig. 4M), decreased the PDT of the respective GSC lines, increased of the 65% number and diameters of GSC colonies in soft agar, and doubled GSC motility (Fig. 4M–4O). Wi38-derived exosomes did not affect any of the three considered parameters. Altogether, these results showed that functional features of tumor-supporting cells characterize GASC and that this effect can be attributable to the release of exosomes.

GASC Features Predict Prognosis in LGG Patients

Since GASC showed: (a) a state of activation that did not change upon in vitro expansion, and (b) a tumor-supporting effect whose magnitude increased with the grade of glioma, we wondered whether GASC features could predict the clinical behavior of the tumor. We focused our attention on LGG, since new criteria to prognostically stratify these patients are urgently needed [4, 30, 31]. To evaluate whether GASC could fulfill these expectations, we first identified the GASC-features distinguishing LGG from HGG and we inserted them in a score that was finally tested for its capacity to prognostically stratify

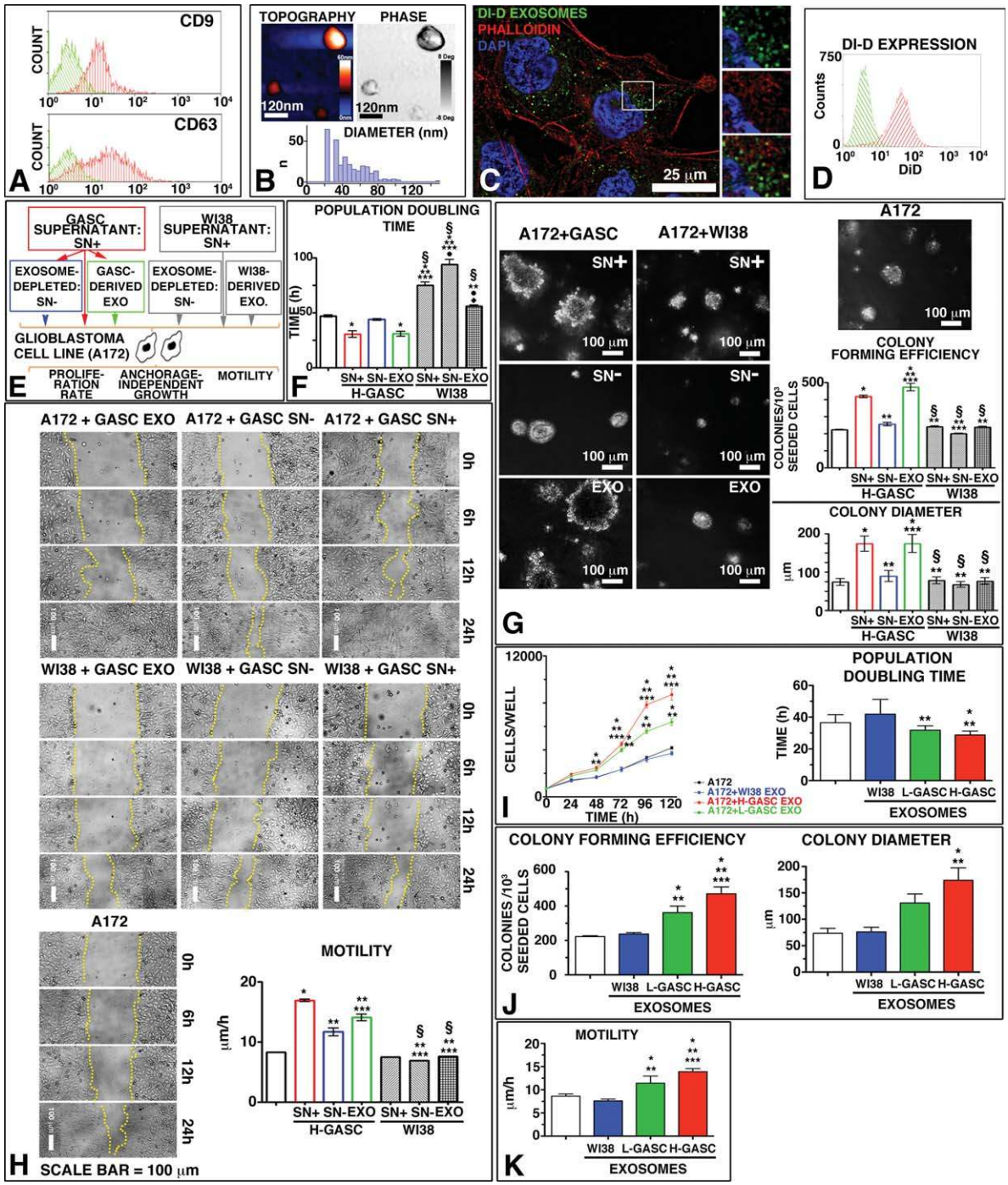

Figure 4. GASC exert their tumor-supporting function through the release of exosomes. **(A):** Histograms overlays showing isotype control IgG staining profile (green histograms) versus specific antibody staining profile (red histograms). **(B):** Upper panels: atomic force microscopy topographic height and phase images of GASC-derived exosomes. The exosomes appear as circular structures with diameters ranging from 20 to 120 nm, and a distinct phase contrast with respect to the surrounding mica surface. Bottom panel: size distribution (diameter in nm) of exosomes ($n = 308$) resulting from the analysis of several atomic force microscopy topographic images. **(C):** DiD-labeled exosomes (green fluorescence) appear to be on the same focal plane of phalloidin-labeled actin filaments (red fluorescence). The area in the inset is presented at higher magnification in the separated and merged panels on the right. Nuclei are depicted by the blue fluorescence of DAPI. **(D):** Histograms overlays showing A172 cells cultured (red histogram) or not (green histogram) with Di-D-labeled exosomes. **(E–G):** Effects of exosomes derived from H-GASC and WI38 on A172 cells. (E): Layout of the experiment. In (F), (G), and **(H)**, results are expressed as mean ± SD. *,**, ***, §, ○, ◇, $p < .05$ versus A172 grown in the absence of exosomes or in the presence of SN+GASC, SN−GASC, EXO-GASC, SN+WI38, and SN−WI38, respectively. (G) Anchorage-independent growth: representative phase-contrast images of colonies of A172 cells grown for 3 weeks in soft agar in the different experimental conditions. (H): Cell motility (scratch assay): representative pictures, taken at different time points, of A172 cells grown in the different experimental conditions. Yellow lines depict the edges of the scratch. **(I–K):** Effects of L-GASC and H-GASC on A172 cells. Results are expressed as mean ± SD. *,**, ***, $p < .05$ versus A172 grown in the absence of exosomes, in the presence of L-GASC- or H-GASC-derived exosomes, respectively. **(L–N):** Effects H-GASC- and WI38-derived exosomes on glioma-initiating stem cell (GSC). (L): Layout of the experiment. (M): Growth kinetic: phase-contrast images of GSC grown either in the absence (i) or in the presence of WI38-derived (ii) and GASC-derived (iii and iv) exosomes. Representative growth curve of a GSC line treated or not with GASC- or WI38-exosomes (v). Population doubling time of GSC treated or not with either GASC-derived or WI38-derived exosomes (vi). Results are expressed as mean ± SD. *,**, $p < .05$ versus A172 grown in the absence of exosomes or in the presence of WI38 exosomes, respectively. (N): Soft agar assay: representative pictures, taken 7 days after seeding, of a GSC line treated or not with GASC- or WI38-derived exosomes. **(O):** Cell motility (scratch assay): representative pictures taken at different time points of a GSC line grown in the different experimental conditions. Yellow lines depict the edges of the scratch. In (M), (N), and (O), results are expressed as mean ± SD. Abbreviation: GASC, glioma-associated stem cells.

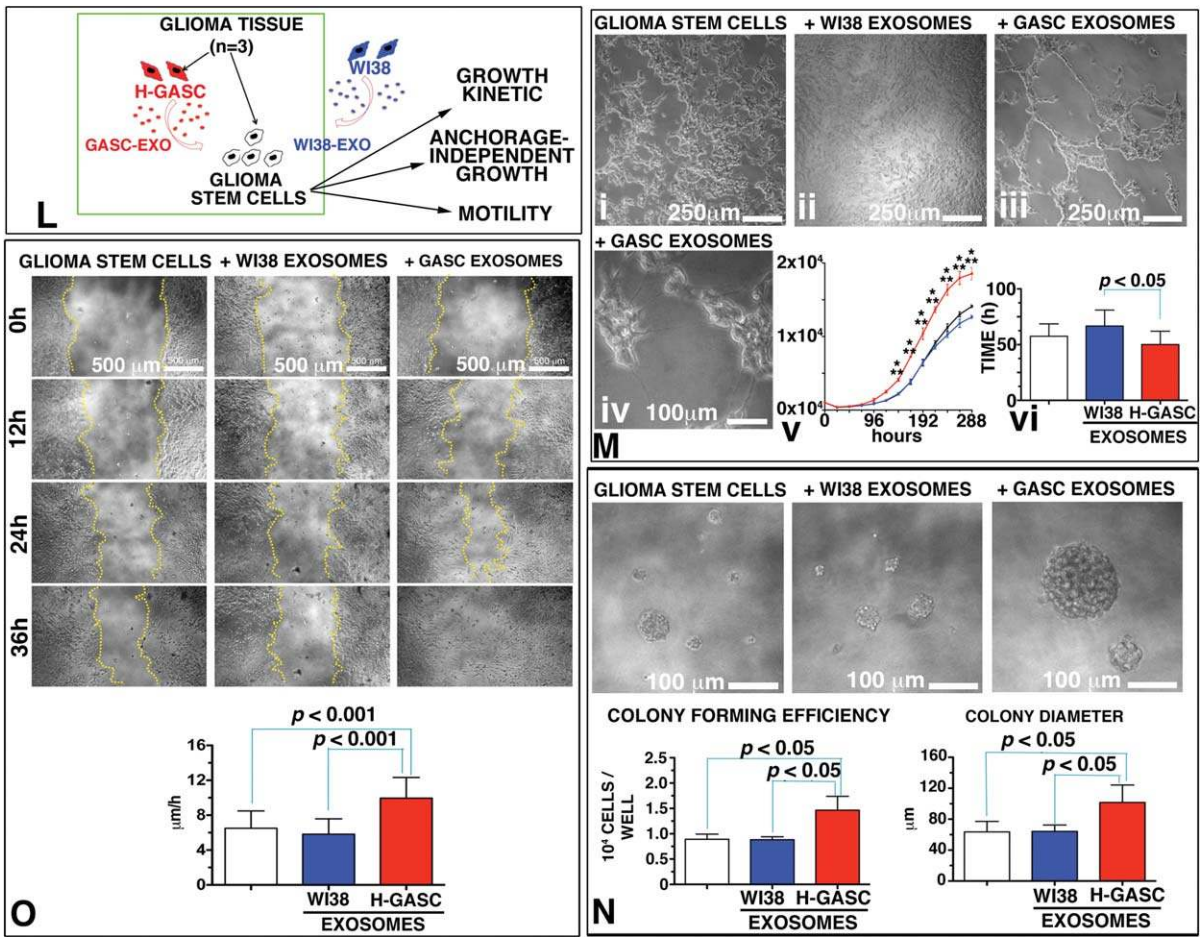

Figure 4. (Continued).

40 LGG patients in terms of OS, MPFS, and PFS (Supporting Information Fig. S1).

Definition of the GASC-Based Score

Starting from a case study composed of 13 H-GASC and 12 L-GASC, obtained, these latter, from patients with an OS >36 months and without MRI evidence of malignant progression, and using De Long's nonparametric receiver operating characteristic (ROC) analysis, we selected nine parameters significantly ($p < .005$) able to correctly classify the two groups and we determined the cut-off value able to discriminate the two populations (Supporting Information Table S4). Of the nine parameters, five were more expressed (CD133, CD271, ABCG2, E-Cadherin, and CD90) and four less expressed (CD49a, CD49d, CD105, and CD73) in H-GASC with respect to the L-GASC, and we expressed the selected parameters as binary values creating a score based on the sum of these latter (Fig. 5A). Finally, we assessed the prognostic value of the determined parameter in a larger casistic including 40 subsequent LGG-patients (median follow-up 36 months, range 13–76) (Table 2).

As illustrated in Figure 5B, eight of the LGG patients presented a score = 0, 10 a score = 1, 14 a score = 2, 1 a score = 3, 2 a score = 5, 1 a score = 6, 2 a score = 7, and two a score = 8. We decided, then, to stratify the score in the following four classes: A (score = 0), B (score = 1), C (score = 2), and D (score >2).

Evaluation of the Prognostic Value of the GASC-Based Score

Table 2 summarizes the demographic, clinical, and histological data of the 40 LGG patients analyzed.

Overall Survival

Overall, there were 12 deaths (30%) and the median follow-up in the surviving patients was 41 months (range 19–76 months). The estimated 5-year OS rates were 100% (score = 0), 90% (score = 1), 42% (score = 2), and 0% (score >2), respectively (log-rank test: $p < .0001$, Fig. 5C).

As summarized in Table 3, the prognostic factors positively associated with OS at univariate analysis ($p < .05$) were the extent of tumor resection (EOR) and the presence of mutated IDH1 or IDH2 genes, while OS was significantly poorer in older patients. Importantly, the GASC-based score was associated with a worse OS, either when treated in its original form or in four classes. Finally, the multivariate Cox analysis showed that the four classes GASC-based score was the only independent predictor of OS (HR 8.84, CI 95% 2.15–36.28, $p = .002$).

Tumor Progression and Malignant Transformation

Tumor progression was identified in 25 (62.5%) cases, while malignant progression was observed in 17 (42.5%) cases. The estimated 2- and 5 years PFS rates were 87.5% and 43.7% (score = 0), 80% and 0.0% (score = 1), 66.7% and 0.0%

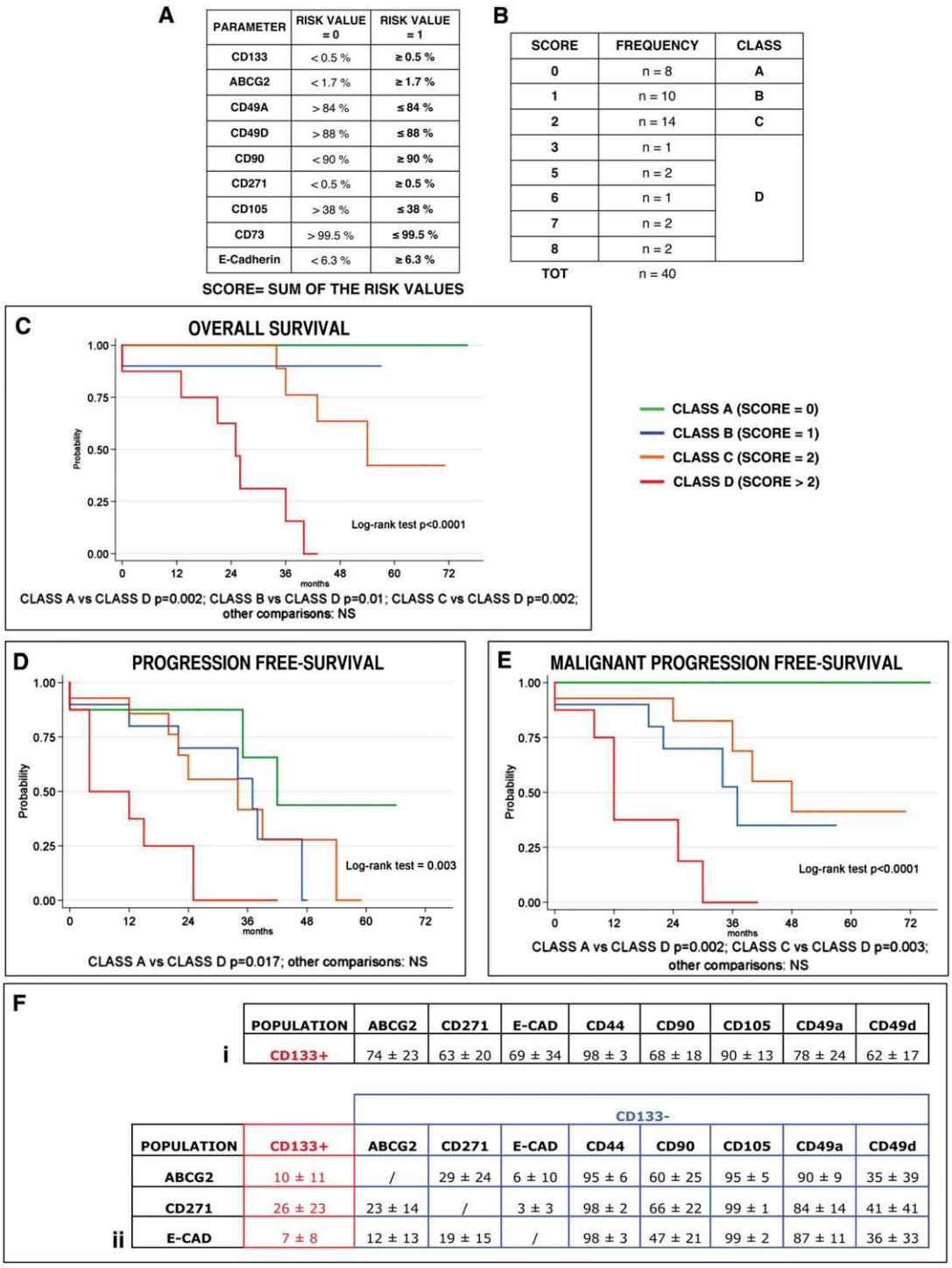

Figure 5. Glioma-associated stem cells (GASC)-based score. **(A–E):** Prognostic value of the GASC-based score in low-grade gliomas (LGG) patients. (A): Parameters and cut-off value used to define the GASC-related score. (B): Distribution of the LGG patients in the in four GASC-classes, according to the GASC-score value. (C–E): Kaplan-Meier curves showing OS (C), PFS (D), and MPFS (E) in LGG patients stratified according to the GASC-based score. **(F):** Populations identified by the parameters included in the GASC-based score. Percentage of $CD133^+$ cells expressing CD44 and the other markers included in the score (i). Fraction of $ABCG2^+$, $CD271^+$, and E-Cadherin $(ECAD)^+$ cells expressing CD133 (ii, on the left) and characterization of the $ABCG2^+/CD133^-$, $CD271^+/CD133^-$, and E-Cadherin $(ECAD)^+/CD133^-$ cells (ii, on the right). Results are expressed as mean ± SD.

(score = 2), and 25% and 0% (score >2), respectively (log-rank test: $p = .003$, Fig. 5D).

At the univariate analysis (Table 3) the EOR was associated with a significant improvement in PFS as well as the presence of mutated IDH1 or IDH2 genes. Again, the GASC-based score was associated with a worse PFS. Finally, the multivariate Cox analysis showed that the only independent predictor of PFS was EOR (HR 0.96, CI 95% 0.93–0.98, $p = .003$). Considering

Table 2. Clinicopathologic features of the $n = 40$ low-grade-glioma patients

Clinicopathologic features	Patients, no.	%	Median (range)
Sex			
Male	25	62.5	–
Female	15	37.5	–
Age at surgery (years)	–	–	38.5 (18–63)
Extent of resection (%)	–	–	88 (25–100)
Tumor subtype			
Astrocytoma	26	65	–
Oligoastrocytoma+ Oligodendroglioma	14	35	–
KI67 expression (%)			5 (1–20)
≤4	18	45	–
>4	22	55	–
P53 expression ($n = 37$)	29	78	–
IDH1 mutation ($n = 35$)	28	80	–
IDH2 mutation ($n = 35$)	2	5.7	–
IDH1 or IDH2 mutation ($n = 35$)	30	85	–
Chromosome 1P deletion ($n = 30$)	10	33	–
Chromosome 19Q deletion ($n = 30$)	13	43	–
Chromosome 1P and 19Q codeletion ($n = 30$)	10	33	–
MGMT promoter methylation ($n = 31$)	26	84	–
number of mitosis/ 10 high power fields	–	–	1 (0–7)
Postoperative chemotherapy	15	37.5	–
Postoperative radiotherapy	23	57.5	–

the MPFS in the four GASC-based score classes, the estimated 2- and 5 years MPFS rates were 100% and 100% (score = 0), 80% and 35% (score = 1), 92.9% and 41.3% (score = 2), and 37.5% and 0% (score >2), respectively (log-rank test: $p < .0001$, Fig. 5E).

At the univariate analysis (Table 3), EOR, presence of mutated IDH1 or IDH2 genes and methylation of the MGMT-promoter were associated with a significant improvement in MPFS. Conversely, older age and the GASC-based score predicted a worse MPFS. Again, the multivariate Cox analysis showed that the only independent predictor of MPFS was the four classes GASC-based score (HR 3.74, CI 95% 1.60–8.75, $p = .002$). Altogether, these results indicate that the GASC-based score is significantly associated with LGG-OS, -MPFS, and -PFS and represents, among the state-of the art LGG prognostic factors, the strongest independent predictor of OS and MPFS.

Evaluation of the Populations Recognized by Markers Included in the GASC-Based Score

To determine whether the markers included in the score recognize the same GASC population or distinct GASC subpopulations, we set multicolor flow-cytometric assays to assess, in six L-GASC, up to six parameters simultaneously (Supporting Information Fig. S5). For technical reasons we could not include in the analysis CD73, but we inserted CD44, given its importance as a marker of glioma stem cells [37, 41].

With the caution due to the low number of cells analyzed, a large fraction of CD133 positive cells express other markers of stemness, such as ABCG2, CD271, and CD44, and, when present, E-Cadherin (Fig. 5F and Supporting Information Fig. S5). They were also largely positive for CD90, CD105, CD49a, and CD49d. However, the large fraction of E-Cadherin$^+$, CD271$^+$, and ABCG2$^+$ cells were not expressing CD133 and only partly overlapped with each one another, thus identifying putative distinct cell subpopulations, usually highly expressing CD105, CD44, and CD49a and variably expressing CD90 and CD49d (Fig. 5F).

Discussion

Personalized medicine aims at identifying patient- and tumor-specific factors useful both for the prognostic stratification of patients and for the identification of therapeutic options that maximize effectiveness, minimizing treatment-related toxicity [42]. This is especially important in neuro-oncology, given the high morbidity and mortality of brain tumors, the rarity of valuable treatment options, and the possible toxicity of therapy [1, 43]. In this article, we have demonstrated that: (a) human gliomas host a novel population of nontumorigenic stem cells, named GASC, that support tumor growth; (b) the optimized method for GASC in vitro expansion is a robust and highly reproducible model of the stromal compartment of both HGG and LGG; (c) GASC support tumor growth releasing exosomes; (d) both tumor stem cells and tumor-supporting cells can be expanded from HGG; (e) GASC features have a strong prognostic value in LGG. The translational nature of this article imposes us to discuss all the basic research findings and their clinical application. (a) Since 2000, Hanahan and Weinberg have postulated that the non-neoplastic component of tumors plays an active role in tumor biology [15, 16]. However, little is known regarding the presence of non-neoplastic stem cells within tumors. These latter may arise from normal progenitors, in analogy with what occurs in Platelet-Derived Growth Factor (PDGF)-induced gliomas of the adult or neonatal rat, where a small population of neural stem cells are "recruited" into the glioma and are induced to proliferate [44]. Accordingly, Kong's group has isolated from a single glioblastoma patient a stem cell line with some mesenchymal features (GS-MSLC) that showed the ability to influence a GSC line by increasing, in vitro, its proliferation, and, in vivo, the size of the formed tumors via an incremented angiogenesis [45, 46]. Our article newly shows that normal stem cells with mesenchymal features and a wide differentiation potential can be isolated both from LGG and HGG, support tumor growth releasing exosomes, and can predict patient prognosis. (b) The presence of GASC raises issues regarding their origin. There is a limited presence of fibroblasts in the CNS and their proliferation has never been described in the course of pathology [47]. Instead, the cell type that characterizes the CNS' response to injury is represented by reactive astrocytes [48, 49]. Importantly, in murine models, non-neoplastic astrocytes could be converted, by the glioma microenvironment, into a reactive phenotype [50, 51] that could acquire stem cell features similar to GASC [52]. Alternatively, GASC may derive from a recently described population of perivascular mesenchymal stem cells endowed with both mesodermal and neuroectodermal differentiation capacities [53]. However, the identification of the in vivo counterpart of GASC in humans is limited since lineage tracing from the cell-of-origin cannot be done in humans [44]. (c) GASC exert their in vitro tumor-supporting action through the release of exosomes. This finding is in line with recent data from Skog's group, who showed that glioblastoma tumor cells

Table 3. Univariate analysis of clinical, histological and GASC-based parameters with OS, PFS, and MPFS in 40 patients with low-grade-gliomas

	OS			PFS			MPFS		
Covariates	**HR**	**95% CI**	***p***	**HR**	**95% CI**	***p***	**HR**	**95% CI**	***p***
Age (modeled as continuous variable)	1.05	1.00–1.09	**.032**	1.02	0.99–1.052	.182	1.04	1.00–1.08	**.038**
Gender (female vs. male)	0.41	0.11–1.51	.180	0.83	0.36–1.91	.663	0.55	0.19–1.57	.265
% EOR (modeled as continuous variable)	0.97	0.94–0.99	**.015**	0.96	0.94–0.98	**<.0001**	0.97	0.95–1.0	**.022**
Tumor subtype Oligoastrocytoma/oligodendroglioma versus fibrillar astrocytoma	1.35	0.43–4.26	.610	0.74	0.31–1.80	.511	0.81	0.28–2.30	.688
% KI67 >4 versus ≤ 4	1.49	0.45–4.99	.516	2.05	0.86–4.86	.104	2.01	0.70–5.73	.193
Number of mitosis (modeled as continuous variable)	1.40	0.93–2.11	.111	1.22	0.88–1.67	.229	1.37	0.99–1.91	.061
IDH1 mutation Yes versus no	0.13	0.04–0.47	**.002**	0.33	0.12–0.86	**.024**	0.24	0.08–0.68	**.007**
IDH2 mutation Yes versus no	1.73	0.22–13.72	.603	0.58	0.08–4.37	.595	0.95	0.12–7.26	.958
IDH1 or IDH2 mutation Yes or no	0.11	0.03–0.40	**.001**	0.09	0.02–0.31	**<.0001**	0.12	0.04–0.40	**.001**
P53 Expression Yes versus no	0.59	0.17–2.04	.408	1.25	0.42–3.74	.691	0.86	0.27–2.70	.795
MGMT promoter methylation Yes versus no	0.40	0.07–2.21	.296	0.43	0.13–1.36	.149	0.21	0.06–0.80	**.022**
Chromosome 1P-deletion Yes versus no	0.37	0.08–1.73	.205	0.33	0.11–1.04	.058	0.25	0.054–1.13	.072
Chromosome 19Q-deletion Yes versus no	0.24	0.05–1.18	.080	0.35	0.12–1.00	.050	0.16	0.03–0.73	**.018**
Chromosome 1P/19Q codeletion Yes versus no	0.37	0.08–1.73	.205	0.33	0.11–1.04	.058	0.25	0.054–1.13	.072
GASC-based score (modeled as continuous variable)	1.85	1.41–2.44	**<.0001**	1.52	1.25–1.87	**<.0001**	1.58	1.30–1.93	**<.0001**
GASC-based score (modeled as categoric variable)	6.52	2.26–18.86	**.001**	1.83	1.18–2.82	**.007**	2.96	1.57–5.60	**.001**

Boldfacing represents statistical significance values are from two-sided tests (Cox regression) and were statistically significant when $< .05$.
Abbreviations: CI, confidence interval; EOR, extent of surgical resection; GASC, glioma-associated stem cells; HR, hazard ratio; MPFS, malignant progression-free survival; OS, overall survival; PFS, progression-free survival.

could release exosomes, containing mRNA, miRNA, and angiogenic proteins, able to act on endothelial cells, possibly favoring the development of a tumor-permissive microenvironment [54]. Accordingly, the proteome and mRNA profiles of exosome closely reflect the oxygenation status of donor glioma cells and patient tumors [55]. Conversely, it has been recently shown that TAF, through the release of exosomes, could induce, in breast tumor cells, the acquisition of a metastatic phenotype [21]. This suggests the existence of a continuous tumor/stroma crosstalk mediated by exosomes. Accordingly, our article shows that GASC can produce exosomes able to influence GSC obtained from the same patient. Interestingly, exosomes can be also released into the bloodstream [54] and act on distant sites taking part to the formation of a premetastatic niche [22]. Therefore, a deeper comprehension of exosome biology will open new avenues for the treatment of neoplastic lesions. (d) Concerning the surface proteins entering in the GASC score, they essentially belong to three classes: stem cell antigens (CD271, CD133, and ABCG2), adhesion proteins (CD49a, CD49d, and E-Cadherin), and mesenchymal markers (CD90, CD73, and CD105). Specifically, GASC obtained from patients with poor prognosis were characterized by an increase in stem cell-related markers, a downregulation in integrin expression, and a variable modulation of mesenchymal markers. When we evaluated, by multiparametric-cytofluorimetric assays, whether these markers identified the same population or distinct subpopulations, we concluded that, while $CD133^+$ cells frequently coexpressed the other stem cell markers CD271, ABCG2, and E-Cadherin, the majority of the $CD271^+$, $ABCG2^+$, and E-$Cadherin^+$ cells did not express CD133, constituting distinct subpopulations. Therefore, the score seems to take into account distinct subpopulations whose specific role in the natural history of glioma deserves future investigations. Nevertheless, CD133 is a well-established, although debated [56], marker of both neural stem cells and glioma-initiating stem cells [11, 12]. Since GASC were devoid of tumor-initiating properties in vivo, we cannot exclude that human gliomas may contain, as in the murine model previously mentioned [44], a small population of neural stem cells. Alternatively, $CD133^+$ cells may derive from a recently described circulating $CD133^+ABCG2^+$ mesenchymal stem cells endowed with neurogenic potential [57]. (e) Despite the lack of class I evidence, surgical treatment is considered the first option in LGG management [4, 5]. However, the aptitude of LGG to infiltrate eloquent areas represents the major limitation in achieving radical resection [30]. The choice between the different postsurgical therapeutic options for LGG patients is still a challenge, because there are not definitive criteria to classify a lesion as at high-risk or low-risk to progress and

side effects of adjuvant treatments are not justifiable in patients at low-risk of relapse/progression [4, 5]. Recently, some advances in defining novel biomarkers able to better classify LGG have been done [58, 59]. IDH mutations and 1p/19q codeletions seem to be independent prognostic markers for OS [59]. The prognostic/predictive role of the methylation of the MGMT promoter is now under investigation, while that of p53 and Ki67 has been questioned [59]. In this article, considering the state-of the art clinical, histological, and molecular LGG prognostic factors, we confirmed the ability of some of these latter to predict OS, MPFS, and PFS. However, in multivariate analysis, the GASC-based score was the only independent predictor of both OS and MPFS, outperforming all the available criteria in stratifying LGG patients and thus allowing a better clinical management [59]. This can prospects the use of this in vitro model of disease both to predict response to therapy and to identify innovative interventions aimed at interrupting the crosstalk between tumor cells and their supporting stroma. Notably, stromal cells are optimal therapeutic targets for their genetic stability and lower potential to develop drug resistance [60].

Conclusion

This article strongly suggests that the isolation of GASC, the study of GASC/GSC model, and of GASC-derived exosomes can: (a) give insights into the biology of gliomas, (b) directly impact the patients' life establishing novel criteria to identify high-risk patients, and (c) provide a useful criterion to direct current therapies or to exploit novel strategies aimed at targeting the tumor stroma.

Acknowledgments

We thank Dr. Christina Vlachouli for in vivo experiments. This work was supported by FIRB Accordi di programma 2011; title: "FIERCE—FInd nEw moleculaR and CEllular targets against cancer." Pr. RBAP11Z4Z9. 2012–2014; FIRB accordi di programma 2011 pr. RBAP11ETKA_007 "Nanotechnological approaches for tumor theragnostic." Programma per la Cooperazione Transfrontaliera Italia-Slovenia 2007–2013. Title: "Identificazione di nuovi marcatori di cellule staminali tumorali a scopo diagnostico e terapeutico"; AIRC five per mille Special program 2011, Pr. 12214. Title: "Application of Advanced Nanotechnology in the Development of Cancer Diagnostics Tools." Project ERC- 7FP SP 2 IDEAS QUIDPROQUO G.A. n. 269051. Title: "Molecular nanotechnology for life science applications: quantitative interactomics for diagnostics, proteomics and quantitative oncology." The funders had no role in study design, data collection and analysis, decision to publish, or preparation of the manuscript.

Author Contributions

E.B. and D.C.: conception and design, collection and/or assembly of data, data analysis and interpretation, manuscript writing, and final approval of manuscript; D.M. and A.Pu.: conception and design, collection and/or assembly of data, data analysis and interpretation, and final approval of manuscript; T.I.: conception and design, provision of study material or patients, collection and/or assembly of data, and final approval of manuscript; M.I. and G.G.: data analysis and interpretation, manuscript writing, and final approval of manuscript; D.M.: collection and/or assembly of data and data analysis and interpretation; S.M., S.P., G.F., and G.D.M.: collection and/or assembly of data and final approval of manuscript; B.T., M.S., A.Pa., F.C., V.P., M.E.R., P.P., and L.C.: collection and/or assembly of data, data analysis and interpretation, and final approval of manuscript; M.V.: provision of study material or patients and final approval of manuscript; G.G.: data analysis and interpretation and final approval of manuscript; G.S.: financial support, data analysis and interpretation, and final approval of manuscript; M.S.: conception and design, financial support, provision of study material or patients, and final approval of manuscript; C.A.B. and A.P.B.: conception and design, financial support, data analysis and interpretation, manuscript writing, and final approval of manuscript. E.B. and D.M. share the first authorship. A.P.B. and D.C. share the last authorship.

Disclosure of Potential Conflicts of Interest

The authors indicate no potential conflicts of interest.

References

1 Wen PY, Kesari S. Malignant gliomas in adults. N Engl J Med 2008;359:492–507.

2 Louis DN, Ohgaki H, Wiestler OD et al. The 2007 WHO classification of tumours of the central nervous system. Acta Neuropathol 2007;114:97–109.

3 Ohgaki H. Epidemiology of brain tumors. Methods Mol Biol 2009;472:323–342.

4 Soffietti R, Baumert BG, Bello L et al. Guidelines on management of low-grade gliomas: Report of an EFNS-EANO task force. Eur J Neurol 2010;17:1124–1133.

5 Duffau H. Surgery of low-grade gliomas: Towards a 'functional neurooncology'. Curr Opin Oncol 2009;21:543–549.

6 Sanai N, Chang S, Berger MS. Low-grade gliomas in adults. J Neurosurg 2011;115:948–965.

7 Bourne TD, Schiff D. Update on molecular findings, management and outcome in low-grade gliomas. Nat Rev Neurol 2010;6:695–701.

8 Stupp R, Tonn JC, Brada M et al. High-grade malignant glioma: ESMO Clinical Practice Guidelines for diagnosis, treatment and follow-up. Ann Oncol 2010;21(suppl 5):v190–193.

9 Vitucci M, Hayes DN, Miller CR. Gene expression profiling of gliomas: Merging genomic and histopathological classification for personalised therapy. Br J Cancer 2011;104:545–553.

10 Salvati M, Pichierri A, Piccirilli M et al. Extent of tumor removal and molecular markers in cerebral glioblastoma: A combined prognostic factors study in a surgical series of 105 patients. J Neurosurg 2012;117:204–211.

11 Singh SK, Hawkins C, Clarke ID et al. Identification of human brain tumour initiating cells. Nature 2004;432:396–401.

12 Galli R, Binda E, Orfanelli U et al. Isolation and characterization of tumorigenic, stem-like neural precursors from human glioblastoma. Cancer Res 2004;64:7011–7021.

13 Pollard SM, Yoshikawa K, Clarke ID et al. Glioma stem cell lines expanded in adherent culture have tumor-specific phenotypes and are suitable for chemical and genetic screens. Cell Stem Cell 2009;4:568–580.

14 Cesselli D, Beltrami AP, Pucer A et al. Human low grade glioma cultures. In: Duffau H, ed. Diffuse Low-Grade Gliomas in Adults. Springer, London, UK, 2013:137–163.

15 Hanahan D, Weinberg RA. The hallmarks of cancer. Cell 2000;100:57–70.

16 Hanahan D, Weinberg RA. Hallmarks of cancer: The next generation. Cell 2011;144:646–674.

17 Place AE, Jin Huh S, Polyak K. The microenvironment in breast cancer progression: Biology and implications for treatment. Breast Cancer Res 2011;13:227.
18 Cirri P, Chiarugi P. Cancer-associated-fibroblasts and tumour cells: A diabolic liaison driving cancer progression. Cancer Metastasis Rev 2012;31:195–208.
19 Gonda TA, Varro A, Wang TC et al. Molecular biology of cancer-associated fibroblasts: Can these cells be targeted in anticancer therapy? Semin Cell Dev Biol 2010;21:2–10.
20 Zhang J, Liu J. Tumor stroma as targets for cancer therapy. Pharmacol Ther 2013;137:200–215.
21 Luga V, Zhang L, Viloria-Petit AM et al. Exosomes mediate stromal mobilization of autocrine Wnt-PCP signaling in breast cancer cell migration. Cell 2013;151:1542–1556.
22 Peinado H, Aleckovic M, Lavotshkin S et al. Melanoma exosomes educate bone marrow progenitor cells toward a pro-metastatic phenotype through MET. Nat Med 2012;18:883–891.
23 Taylor DD, Gercel-Taylor C. Exosomes/microvesicles: Mediators of cancer-associated immunosuppressive microenvironments. Semin Immunopathol 2011;33:441–454.
24 Azmi AS, Bao B, Sarkar FH. Exosomes in cancer development, metastasis, and drug resistance: A comprehensive review. Cancer Metastasis Rev 2013;32:623–642.
25 Thery C, Amigorena S, Raposo G et al. Isolation and characterization of exosomes from cell culture supernatants and biological fluids. Curr Protoc Cell Biol 2006;Chapter 3: Unit 3 22.
26 Simons M, Raposo G. Exosomes–vesicular carriers for intercellular communication. Curr Opin Cell Biol 2009;21:575–581.
27 Charles NA, Holland EC, Gilbertson R et al. The brain tumor microenvironment. Glia 2011;59:1169–1180.
28 Hoelzinger DB, Demuth T, Berens ME. Autocrine factors that sustain glioma invasion and paracrine biology in the brain microenvironment. J Natl Cancer Inst 2007;99:1583–1593.
29 Felsberg J, Wolter M, Seul H et al. Rapid and sensitive assessment of the IDH1 and IDH2 mutation status in cerebral gliomas based on DNA pyrosequencing. Acta Neuropathol 2010;119:501–507.
30 Ius T, Isola M, Budai R et al. Low-grade glioma surgery in eloquent areas: Volumetric analysis of extent of resection and its impact on overall survival. A single-institution experience in 190 patients: Clinical article. J Neurosurg 2012;117:1039–1052.
31 Skrap M, Mondani M, Tomasino B et al. Surgery of insular nonenhancing gliomas: Volumetric analysis of tumoral resection, clinical outcome, and survival in a consecutive series of 66 cases. Neurosurgery 2012;70:1081–1093, discussion 1093-1084.
32 Beltrami AP, Cesselli D, Bergamin N et al. Multipotent cells can be generated in vitro from several adult human organs (heart, liver, and bone marrow). Blood 2007;110:3438–3446.
33 Cesselli D, Beltrami AP, D'Aurizio F et al. Effects of age and heart failure on human cardiac stem cell function. Am J Pathol 2011;179:349–366.
34 Cesselli D, Beltrami AP, Poz A et al. Role of tumor associated fibroblasts in human liver regeneration, cirrhosis, and cancer. Int J Hepatol 2011;2011:120925.
35 Hinze A, Stolzing A. Differentiation of mouse bone marrow derived stem cells toward microglia-like cells. BMC Cell Biol 2011;12:35.
36 Cesselli D, Beltrami AP, Rigo S et al. Multipotent progenitor cells are present in human peripheral blood. Circ Res 2009;104:1225–1234.
37 Brescia P, Richichi C, Pelicci G. Current strategies for identification of glioma stem cells: Adequate or unsatisfactory? J Oncol 2012;2012:376894.
38 Velpula KK, Rehman AA, Chelluboina B et al. Glioma stem cell invasion through regulation of the interconnected ERK, integrin alpha6 and N-cadherin signaling pathway. Cell Signal 2012;24:2076–2084.
39 Weiland A, Roswall P, Hatzihristidis TC et al. Fibroblast-dependent regulation of the stem cell properties of cancer cells. Neoplasma 2012;59:719–727.
40 Kahlert C, Kalluri R. Exosomes in tumor microenvironment influence cancer progression and metastasis. J Mol Med (Berl) 2013;91:431–437.
41 Anido J, Saez-Borderias A, Gonzalez-Junca A et al. TGF-beta receptor inhibitors target the CD44(high)/Id1(high) glioma-initiating cell population in human glioblastoma. Cancer Cell 2010;18:655–668.
42 Hamburg MA, Collins FS. The path to personalized medicine. N Engl J Med 2010;363:301–304.
43 Johnson DR, Galanis E. Incorporation of prognostic and predictive factors into glioma clinical trials. Curr Oncol Rep 2013;15:56–63.
44 Fomchenko EI, Dougherty JD, Helmy KY et al. Recruited cells can become transformed and overtake PDGF-induced murine gliomas in vivo during tumor progression. PLoS One 2011;6:e20605.
45 Kim YG, Jeon S, Sin GY et al. Existence of glioma stroma mesenchymal stemlike cells in Korean glioma specimens. Childs Nerv Syst 2012;29:549–563.
46 Kong BH, Shin HD, Kim SH et al. Increased in vivo angiogenic effect of glioma stromal mesenchymal stem-like cells on glioma cancer stem cells from patients with glioblastoma. Int J Oncol 2013;42:1754–1762.
47 Estin C, Vernadakis A. Primary glial cells and brain fibroblasts: Interactions in culture. Brain Res Bull 1986;16:723–731.
48 Reifenberger G, Szymas J, Wechsler W. Differential expression of glial- and neuronal-associated antigens in human tumors of the central and peripheral nervous system. Acta Neuropathol 1987;74:105–123.
49 Tamagno I, Schiffer D. Nestin expression in reactive astrocytes of human pathology. J Neurooncol 2006;80:227–233.
50 Couldwell WT, Yong VW, Dore-Duffy P et al. Production of soluble autocrine inhibitory factors by human glioma cell lines. J Neurol Sci 1992;110:178–185.
51 Lal PG, Ghirnikar RS, Eng LF. Astrocyte-astrocytoma cell line interactions in culture. J Neurosci Res 1996;44:216–222.
52 Buffo A, Rite I, Tripathi P et al. Origin and progeny of reactive gliosis: A source of multipotent cells in the injured brain. Proc Natl Acad Sci USA 2008;105:3581–3586.
53 Paul G, Ozen I, Christophersen NS et al. The adult human brain harbors multipotent perivascular mesenchymal stem cells. PLoS One 2012;7:e35577.
54 Skog J, Wurdinger T, van Rijn S et al. Glioblastoma microvesicles transport RNA and proteins that promote tumour growth and provide diagnostic biomarkers. Nat Cell Biol 2008;10:1470–1476.
55 Kucharzewska P, Christianson HC, Welch JE et al. Exosomes reflect the hypoxic status of glioma cells and mediate hypoxia-dependent activation of vascular cells during tumor development. Proc Natl Acad Sci USA 2013;110:7312–7317.
56 Wan F, Zhang S, Xie R et al. The utility and limitations of neurosphere assay, CD133 immunophenotyping and side population assay in glioma stem cell research. Brain Pathol 2010;20:877–889.
57 Nichols JE, Niles JA, Dewitt D et al. Neurogenic and neuro-protective potential of a novel subpopulation of peripheral blood-derived CD133+ ABCG2+CXCR4+ mesenchymal stem cells: Development of autologous cell based therapeutics for traumatic brain injury. Stem Cell Res Ther 2013;4:3.
58 Riemenschneider MJ, Jeuken JW, Wesseling P et al. Molecular diagnostics of gliomas: State of the art. Acta Neuropathol 2010;120:567–584.
59 Weiler M, Wick W. Molecular predictors of outcome in low-grade glioma. Curr Opin Neurol 2012;25:767–773.
60 Snuderl M, Batista A, Kirkpatrick ND et al. Targeting placental growth factor/neuropilin 1 pathway inhibits growth and spread of medulloblastoma. Cell 2013;152:1065–1076.


See www.StemCells.com for supporting information available online.

